

České vysoké učení technické v Praze  
Fakulta jaderná a fyzikálně inženýrská  
Katedra fyziky

Heat conduction in the divertor target plate of the  
ITER tokamak

(Vedení tepla v divertorové desce tokamaku ITER)

Bakalářská práce

Vedoucí práce: Mgr. Jan Horáček, PhD, ÚFP AV ČR

Autor práce: Alexander Wolff

2010/2011

# Zadání Bakalářské Práce

## Prohlášení

# 1 Abstract and Keywords

The temperature of the divertor target of a tokamak partially implicates the rate of material (graphite or Tungsten) eroded from its surface and therefore its lifetime. The main problem at the future international experiment ITER will be the large heat and particle fluxes at the creation of giant Edge Localized Modes (ELMs). The damage done by these can cause expensive reconstructions and long interruptions of operation.

The simulation, which this work is concerned with, is built on a Matlab/Octave code from Mgr. Jan Horáček, PhD and was adapted for the divertor strike point of the ITER tokamak. It numerically solves the equations, describing the heat conduction within the material. As input data serve the material constants (heat capacity, conductivity and density) of CFC and Tungsten, the time dependent flux during ELM events from a PIC simulation [2], and the spacial distribution from a model [3] developed at the Institute of Plasma Physics (IPP) in Prague.

This work compares Carbon-Fiber-Composite (CFC) and Tungsten in order to assess, which material is more suitable for the DT-phase of the ITER operation. The code takes into account active cooling, gray body radiation as well as sublimation and melting. Not considered are physical and chemical erosion.

From the CFC tile 0.17 pg (only a 1 nm layer) are eroded through sublimation during one ELM. No Tungsten from the tile melted. A divertor made from Tungsten takes no damage from thermal erosion. Further advantages are lower chemical and physical erosion [1]. This means, that a divertor made only from Tungsten should be a realistic option for ITER.

This conclusion does not correspond to the pessimistic estimations from literature [1]. Since our model was successfully cross checked against the analytical solution of surface heating, this quite puzzling. The main question must now be, if the input data is responsible for this or if the fear of a rapid divertor destruction due to ELMs is unjustified.

Keywords (English):

Heat conduction, thermonuclear fusion, plasma, divertor, ITER, Edge Localized Mode, ELM, Simulation, Tungsten, Carbon Fiber Composite, CFC

Keywords (Czech) – klíčová slova:

Vedení tepla, plazma, termojaderná fúze Divertor, ITER, ELM, Wolfram, CFC

# Content

Zadání Bakalářské Práce.....	2
Prohlášení.....	3
1 Abstract and Keywords.....	4
2 Introduction.....	7
2.1 The Need for Fusion Energy.....	7
2.1.1 Energy Demand.....	7
2.1.2 Resource Availability.....	7
2.1.3 Emissions and Waste.....	8
2.1.4 Nuclear Safety.....	9
2.2 Physics of Fusion.....	10
2.2.1 Fusion in Nature.....	11
2.2.2 Fusion as a Source of Energy.....	12
2.3 Tokamaks.....	14
2.3.1 Basic Principle.....	14
2.4 ITER.....	16
2.4.1 History.....	16
2.4.2 Anatomy.....	16
2.4.3 Demands.....	19
2.4.4 Program.....	20
2.5 Divertor.....	22
2.5.1 General Description.....	22
2.5.2 Components and their Function.....	23
2.5.3 Choice of Armor Materials.....	24
2.6 Edge Localized Modes (ELMs).....	25
3 Simulation of the Heat Conduction.....	26
3.1 Motivation.....	26
3.2 Input from other Simulations.....	28
3.3 The Model.....	31
3.3.1 Maths Behind the Model.....	31
3.3.2 Verification of the Model.....	32
3.4 Technical Details of the Program.....	33
3.4.1 Parameters and Observed Quantities.....	33
3.4.2 Boundary Conditions.....	34
3.4.3 Implicated Cooling Mechanisms.....	34
3.4.4 Issues for Simulating Tungsten.....	35
3.4.5 Issues for Simulating CFC.....	36
3.5 Results.....	39
3.5.1 Tungsten.....	39
3.5.2 CFC.....	41
3.5.3 Comparison.....	43
3.6 Summary.....	44

3.7 Implications.....	45
3.8 Possible Future Improvements.....	46
4 References.....	47
5 Acknowledgments.....	49

## 2 Introduction

### 2.1 The Need for Fusion Energy

#### 2.1.1 Energy Demand

Several factors indicate that the demand for energy in the future is going to rise dramatically. World population is expected to grow to 8.1 billion people by 2030 [11] and to over 10 billion by the end of the century. This rise in population alone requires an increase in energy supply.

Secondly the industrialization of less developed countries and the improving standard of living in countries such as China, further increase the demand for energy.

Adding these factors together this means that the consumption of energy (if met by supply) is going to increase drastically in the next decades (see Figure 1).

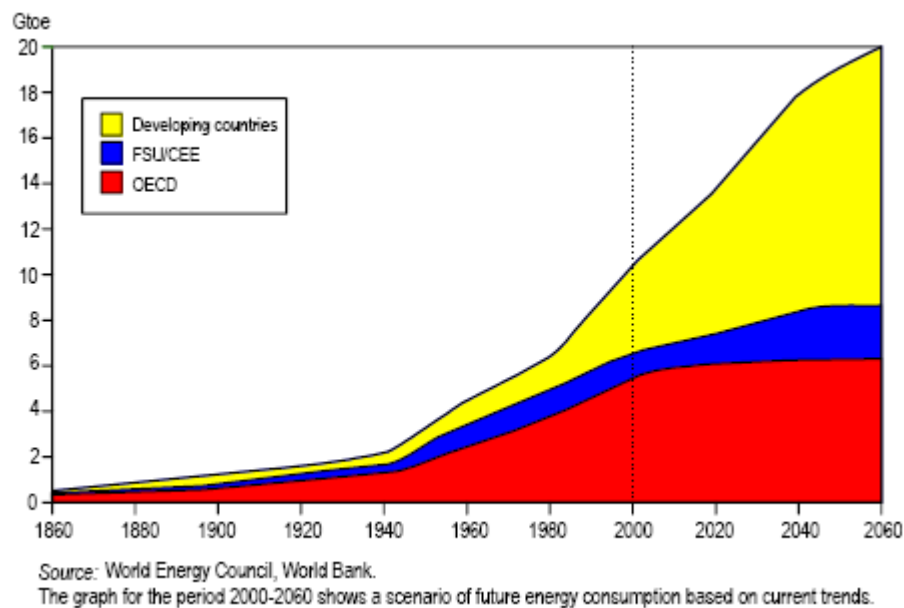


Figure 1: Projection of future energy demand [11]

#### 2.1.2 Resource Availability

At the current rate of resource consumption, oil is expected to run out before the end of the 21<sup>st</sup> century. Estimates of how long oil will last, go as low as 30 years. [11] Coal as the most

common source for electrical energy is supposed to run out in about 120 years. However, since these estimates usually take into account only known reserves, the real time these resources could be available will most likely be longer. Especially oil reserves have still been discovered in the last decade.

To a certain extent also nuclear power faces trouble due to fuel (Uranium) shortage. At the current rate of use, Uranium is expected to run out in less than 100 years. [11,12] The development of breeder reactors, however means that nuclear fuel can be used much more efficiently and last substantially longer [11,12]. There are also options of extracting Uranium from sea water [13], which currently is not an economically efficient process due to its low concentration. Rising energy prices could change that.

There still remains the need for a long term solution for covering the world's energy demand. Renewable energy sources are already available, but their usage is often limited by geographical conditions. Solar and wind power depend on the weather and a constant operation cannot be guaranteed.

Fuel for fusion reactors is widely available. Deuterium can be gained from water. 1 in 6700 Hydrogen atoms in water are actually Deuterium. That means that 1litre of water contains 0.033 g of Deuterium and an energy equivalent of 10GJ (same as 280 l of oil). Hence Deuterium could be used to supply energy for billions of years. Tritium on the other hand does not occur in nature, due to its short half life (12.3 years). It can however be gained from Lithium, through neutron bombardment. The known Lithium reserves would last for thousands to millions of years [11].

### **2.1.3 Emissions and Waste**

In order to reduce the effects of global climate change, Carbon emissions need to be reduced and energy production therefore needs to be decoupled from fossil fuels [11]. This requires a reliable large scale energy source. Fission can take this role only to a limited extent, as there are also political (and global safety) issues attached to uranium enrichment. Another issue is the production (and storage) of radioactive waste.

Fusion energy does not produce CO<sub>2</sub> and the Tritium produced on site gets used as fuel again. There is no need for long term storage. However the reactor vessel itself can be activated through high neutron fluxes. Research into low activation materials suitable for

fusion reactors should help to reduce this problem.

#### **2.1.4 Nuclear Safety**

At a fusion power plant much less radioactive material (several grams of Tritium) is stored than at a fission reactor (kilograms of Uranium or other reactor fuel). A fusion reaction can only occur under controlled conditions, even a burning plasma (self heating through fusion products), would quickly run out of fuel. A runaway chain reaction is not possible, since any contact between the fusion plasma and its surrounding wall would cause a great amount of impurities to radiate of all the energy in the plasma and thus stopping any further reaction.

## 2.2 Physics of Fusion

Fusion is the change of two light nuclei into a heavier one. For atoms lighter than iron (Fe56) this reaction releases energy (see Figure 2). In each nucleus some mass of its nucleons is converted to energy when the nucleus forms. This is due to the strong force acting between nucleons within a nucleus. The energy can be passed on to other particles through collisional interaction.

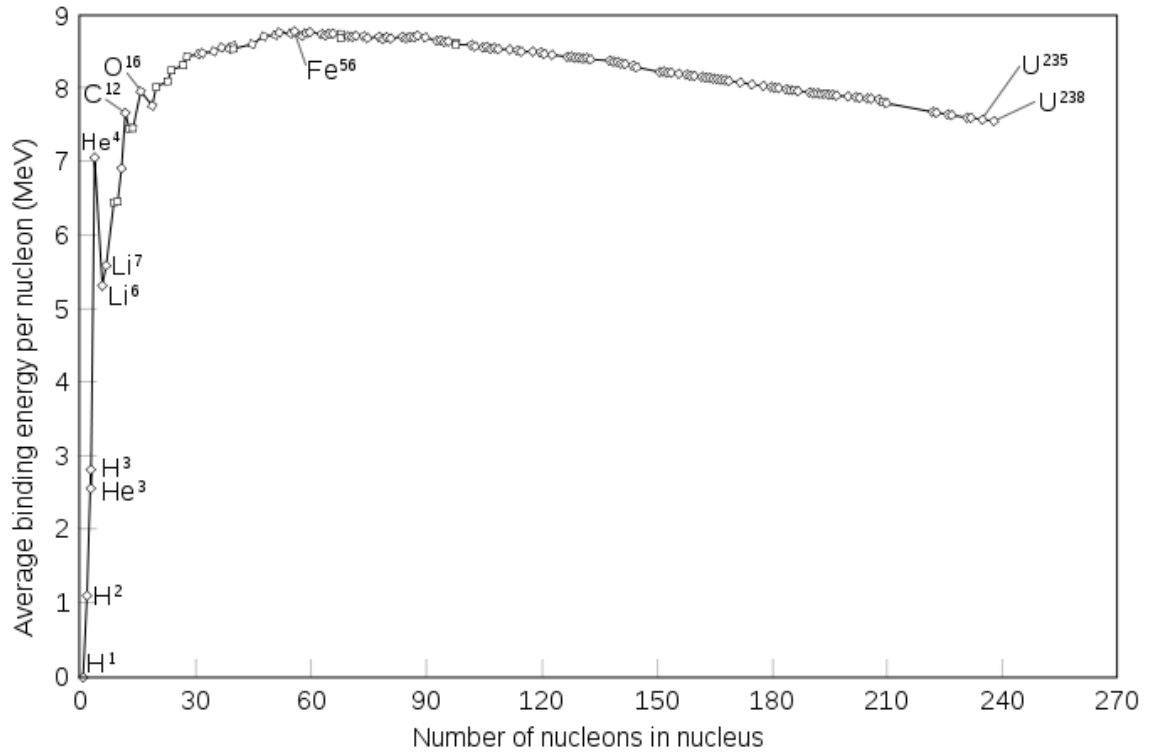


Figure 2: The nuclear binding energy is equal the energy required to take apart a nucleus into single protons and neutrons. Dividing by the number of nucleon in the nucleus gives an overview of how strong the bonds within are. Fe-56 has the highest binding energy per nucleon. Energy can be gained through fusion if the resulting element is lighter than iron-56 or through fission if the products are heavier than iron. [9]

Before two nuclei can fuse they have to overcome the Coulomb force acting between those two positive particles. Only when they approach close enough for the strong force to become dominant, fusion can take place. In order to make Deuterium and Tritium nuclei to come that close the need to have kinetic energies corresponding to the potential of the Coulomb barrier (see Figure 3). The energy release through the fusion products on the other hand corresponds to the potential difference between the Coulomb barrier and the bottom of the strong force well.

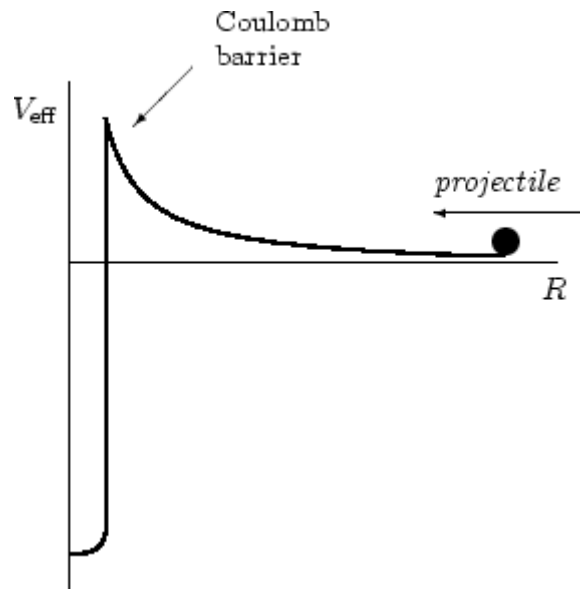


Figure 3: Coulomb barrier and strong force well [18]

### 2.2.1 Fusion in Nature

Our universe, as we know it, is a result of fusion. All heavy atoms were created through fusion because during the “Big Bang” only elementary particles were created. The conditions on earth are mainly due to energy we receive from the sun. In the sun fusion is kept up as a chain reaction (as long as its fuel will last). The high pressure and temperature inside the core secure the conditions to overcome the energy barriers for the reactions. The reactions then further heat up the plasma in the sun. Fusion occurs in all stars. The type of fusion reaction depends on the size and age of a star.

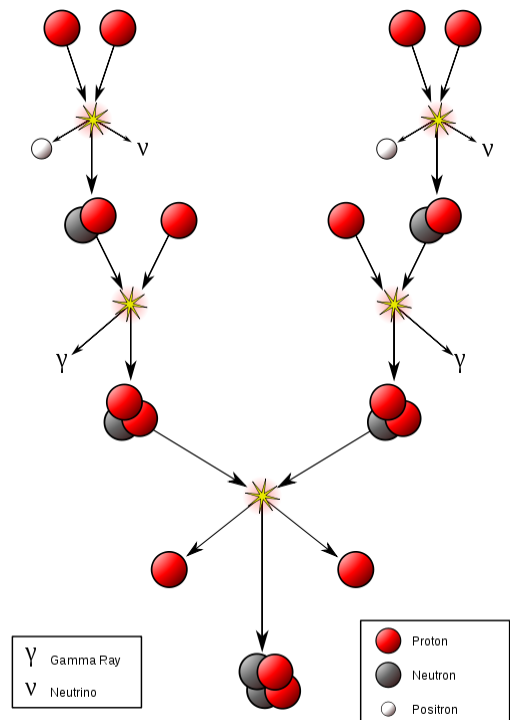


Figure 4: Proton-Proton chain [5]

The reactions taking place in the sun are known as the proton-proton chain (see Figure 4).

4 Hydrogen ions fuse into 2 Deuterium nuclei emitting 2 positrons and 2 neutrinos with a net

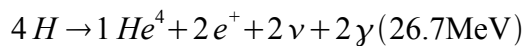
energy release of 0.42 MeV.

The positron annihilates with one of the electrons present in the plasma to release another 1.02 MeV.

Deuterium fuses with another Hydrogen to form Helium-3 with the emission of a gamma ray. This reaction releases 5.49 MeV.

There are several reactions to produce Helium-4 from Helium-3. Which of them occurs depends largely on the temperature of the plasma they occur in.

Independent on the reaction path the formation of Helium-4 from 4 protons releases 26.7 MeV of energy.



In our sun only Helium is regularly created. For other reactions creating heavier elements the sun is not sufficiently massive. These reactions occurring in other more massive stars are not relevant for fusion research on earth. [5]

### 2.2.2 Fusion as a Source of Energy

There are two basic approaches to get fusion energy. One is magnetic confinement, the other one inertial fusion.

In magnetic confinement large magnetic fields are used to keep the charged particles of the plasma on helical orbits, while inertial fusion requires a quick heating of the fusion fuel, using lasers, before it can expand.

Fusion energy can be obtained on earth fusing Deuterium with Tritium, releasing a 14.1 MeV neutron and a 3.5 MeV alpha particle or fusing two Deuterium ions into Tritium and a proton or into Helium-3 and a neutron. Both D-D reactions are equally probable at the D-D cross-section peak. However the cross-section of the D-T reaction is 100 times bigger (see Figure 5) at the temperatures currently worked with in

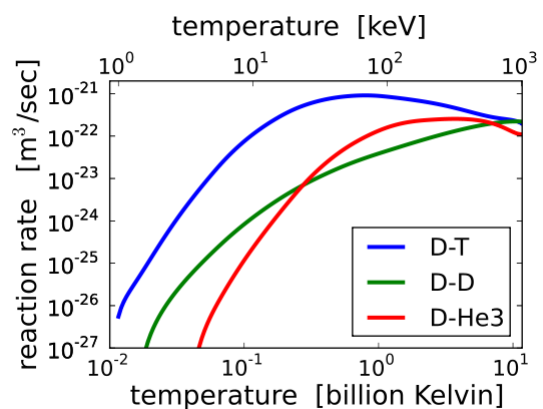


Figure 5: Reaction rates of fusion reactions at temperatures around 100 million K [5].

fusion research (150 million K for ITER).

In a magnetically confined plasma, the neutrons produced in these reactions are not affected by the magnetic field. They leave the plasma immediately and their energy can be used to heat water and thus power a steam turbine.

The target in fusion research is to get as close as possible to a so called burning plasma, where all the heating is done by the energy of the charged products of the fusion reactions. For such a plasma the Lawson criterion resp. Triple product (1) needs to be fulfilled.

$$n_e T \tau_E \geq 10^{21} \text{ keV s/m}^3, \quad (1)$$

Two of the three parameters are relatively hard to increase. The density  $n_e$  of the plasma is limited by the magnetic pressure, which the external magnetic field can provide. The temperature  $T$  of the plasma needs to be kept within reasonable boundaries to get favorable cross-sections for the desired fusion reactions (see Figure 5). This means that the energy confinement time  $\tau_E$  is the main factor determining the success of achieving a burning plasma. Ways to achieve a better  $\tau_E$  are for example better shaping of the tokamak plasma or finding improved modes of operation.

## 2.3 Tokamaks

One option for controlled fusion is magnetic containment inside a tokamak. A tokamak is a torus shaped device, that generates a large magnetic field inside itself to control the plasma. Tokamak plasmas have a low density and a very high temperature (hotter than the core of the sun). Tokamaks were first designed and operated in the Soviet Union in 1956.

### 2.3.1 Basic Principle

The fuel for tokamak fusion experiments is Deuterium and Tritium. Fusion using only deuterium is also considered, but due to the 100 lower cross-section of the reaction and its lower yield this is not at the stage where energy can be gained.

Gaseous fusion fuel is fully ionized and turned into a plasma. The plasma is then heated (inductively and from external sources) to a temperature of over one hundred million Kelvin, which is many times higher than the temperature in the core of the sun. No material would withstand such heat, so the plasma has to be kept away from the walls of the torus. This done with a big magnetic field. In the toroidal direction (see Figure 6, top) a large magnetic field (several Tesla) is applied. The Lorentz force then keeps all charged particles on helical orbits around the field lines. Particles can leave this confinement through drifts but also through collisions between each other. To reduce

this effect, a poloidal field is used to twist (Figure 6, bottom) the field lines. The main component of the poloidal field is coming from the plasma current (Figure 6, middle). This way the drifts felt by the particles are canceling themselves. To protect the torus wall, older

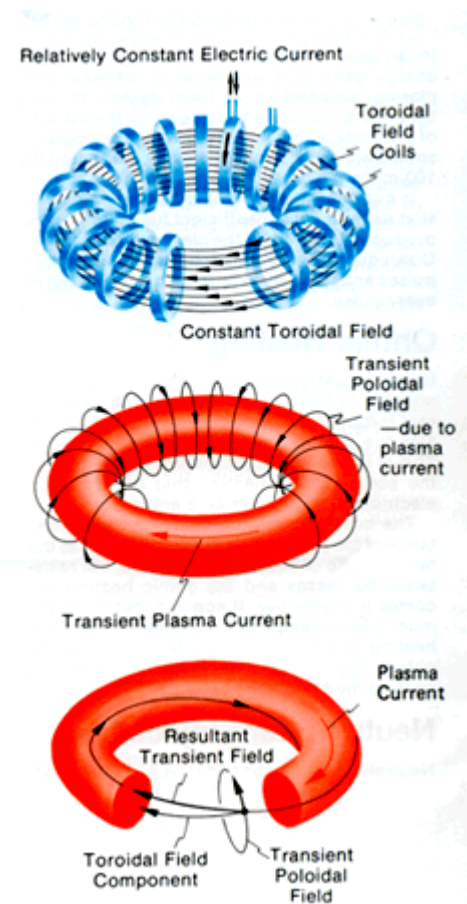


Figure 6: Generation of the magnetic field in a tokamak

tokamaks had so called limiters. Limiters are basically elevations of the wall, made of a more resilient material. Between the limiter columns the wall does not get much contact to the plasma. Modern big tokamaks however work with a divertor. The outer poloidal field lines are opened in one place and all particles following them are directed away from the main plasma onto targets made of materials specially suited for such high loads. This way the contact of the plasma with the chamber is localized to the strike points.

Tokamaks have greatly improved over the years and are considered the best option for controlled fusion at the moment. To prove this, a new big tokamak is currently built: ITER

## **2.4 ITER**

ITER is an international project for building a long pulse tokamak. It is financed by the European Union, USA, Russia, India, China, Japan and South Korea. When construction will finish in 2018 [14], it will be the largest tokamak in the world. It should be able to achieve 500MW of DT fusion power for a pulse length of 400s. Only 50MW of auxiliary input power are planned, meaning a Q of 10.

Its main objective is to show that gaining energy from fusion is possible and solve the scientific and engineering problems standing in the way of construction a fusion power plant. ITER will research into improved control of the plasma and reactor related materials. Its planned successor (DEMO) will take advantage of this research and be the first prototype of a power plant.

### **2.4.1 History**

The agreement to design ITER (International Thermonuclear Experimental Reactor) was signed in 1986 between the USA, USSR, EU (through EURATOM) and Japan. The design was worked out from 1988 to 1990 and a final design was accepted in 1998. Due to high costs the USA terminated their participation in the same year.

However the design was changed in 2001 in order to cut the costs to 50%, while still being able to implement the programmatic plans. In 2003 China and Korea joined the project and the US returned to it. After India joining in 2005, more than half of the world's population are represented by the 7 ITER parties. [14]

The preparation of the site in Cadarache, France began in 2007, construction started in in 2010. Operations are due to start in 2019 [14].

### **2.4.2 Anatomy**

An overview of the ITER machine can be seen on Figure 7.

The main components of the ITER machine are the vacuum vessel, the superconducting magnets, the blanket and the divertor, as well as the cryostat, external heating systems and the diagnostics (numbered in this order on Figure 7). [14]

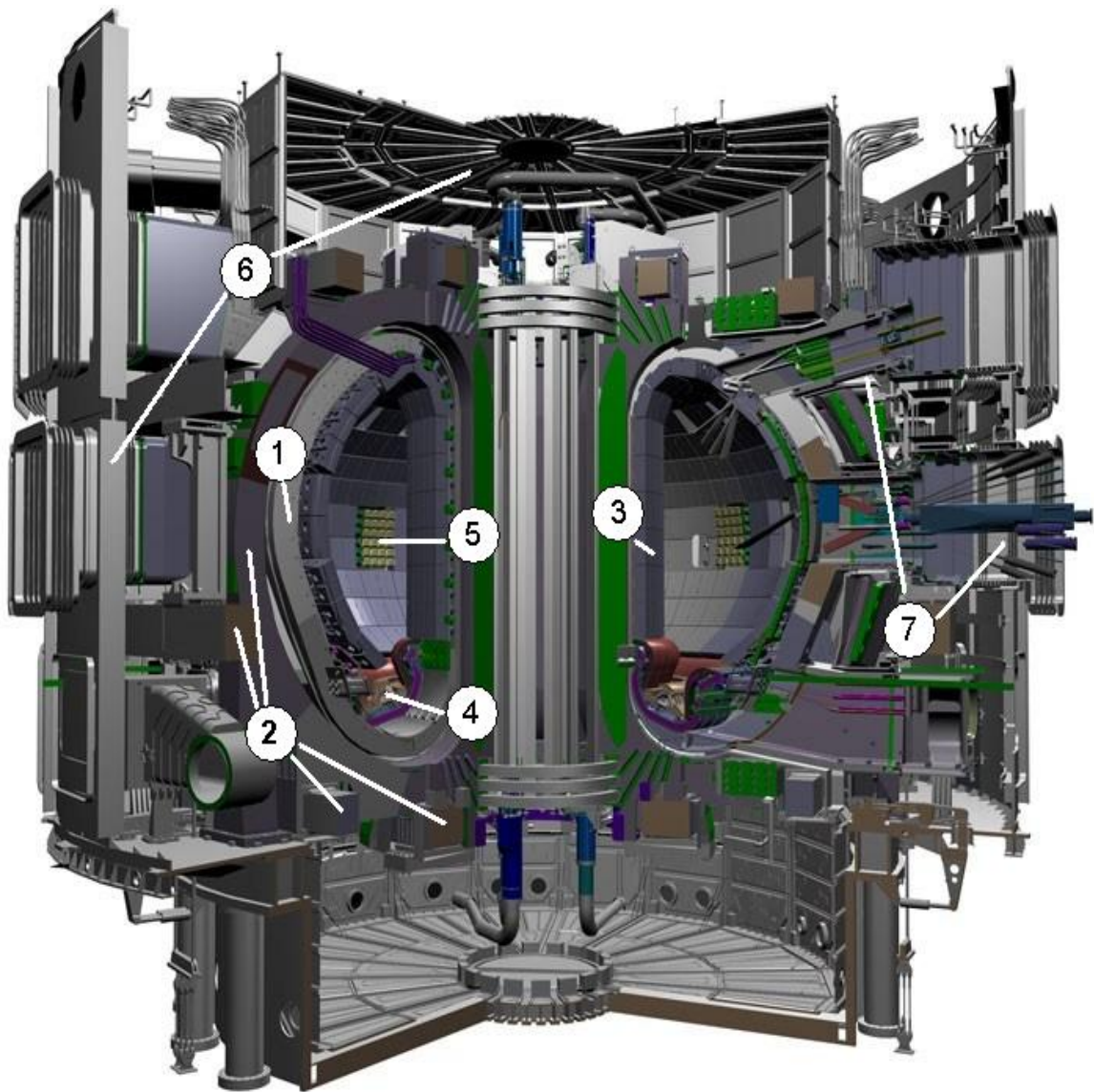


*Figure 7: Overview over ITER [17], highlighting the 1) vacuum vessel, 2) magnets, 3) blanket, 4) divertor, 5) external heating, 6) cryostat and 7) diagnostics [14]*

The vacuum vessel is a double walled stainless steel container in the shape of a torus. Its outer diameter is 19 m, its height 11 m. The inner diameter is 6 meters. The vessel will be welded together from 9 parts. Between the walls there will be water cooling and from the inside it will be protected from high energy neutrons by the blanket modules. The vessel will have 44 ports [14] providing access for remote handling, diagnostics, external heating and the vacuum pumps.

The ITER magnet system consists of 18 (superconducting) Toroidal Field (TF) coils,

6 Poloidal Field (PF) Coils, a central solenoid and several correction coils.

The TF magnets produce an up to 11.8 Tesla magnetic field around the chamber, confining the plasma within it. The magnetic energy will be up to 41 GJ [14]. To achieve such high values the magnets need to be cooled to the point where they become superconducting. These coils will be mounted closely around the vessel.

The PF will be induced by the plasma current and by the 6 horizontal PF coils. The poloidal component of the magnetic field causes the field lines to twist around the chamber counteracting negative effects of drifts, thus improving confinement. The PF coils will be mounted around the TF coils.

The central solenoid can be viewed as a large transformer. It stands in the center of the tokamak and is made of 6 independent coils and serves the purpose of current drive, but also helps to shape the field in the divertor region [14].

The blanket provides shielding to the vessel and the magnets behind it from high heat and neutron loads. For easier maintainability it is made of 440 [14] modular segments, that can be serviced individually through remote handling. Its detachable first wall is made of Beryllium and serves the purpose of heat absorption from the plasma. The underlying blanket is made of copper and stainless steel. It serves the slowing and absorption of neutrons. The energy released by the neutrons is collected by coolants. In a power plant this coolant would power the turbines of the generators.

The divertor is made of 54 cassettes [14,15,16], each serviceable individually through remote handling. It is located at the bottom of the vessel and will have to withstand high heat loads and particle fluxes. Chapter 2.5 is dedicated to the divertor in detail.

The external heating consists of several systems: Neutral Beam Injection (NBI) and Ion resp. Electron Cyclotron Resonance Heating (ICRH resp. ECRH).

The NBI accelerates D ions to high (order of magnitude: MeV) energies neutralizes them and fires them into the plasma. Through collisions they “share” their energies with the particles already present in the plasma. They have to be neutral, otherwise they would not be able to cross the magnetic field lines, confining the plasma.

The resonance heating systems send microwaves at the resonant frequencies of 30-50MHz and 100-200 MHz for ions and electrons respectively. This way the particles are accelerated and therefore the plasma heats up.

The cryostat is a large container around the vessel and the magnets providing a vacuum environment at low temperatures. Like the inner vacuum vessel, it has several openings for access. Hot parts are thermally isolated from the cooled magnets.

The diagnostics around ITER serve the purpose of research and control of the plasma behavior. There is a wide variety of technologies applied in the diagnostics, that have to withstand the extreme conditions near the plasma while still operating with maximum precision. There will be about 50 diagnostic systems operating on ITER [14].

### 2.4.3 Demands

The revised performance specifications adopted by the ITER Council in June 1998 in summary require ITER [15,16]:

- to achieve extended burn in inductively-driven deuterium-tritium plasma operation with  $Q \geq 10$ , not precluding ignition, with an inductive burn duration between 300 and 500 s and a range of operating scenarios;
- to aim at demonstrating steady state operation using non-inductive current drive with  $Q \geq 5$ ;

In terms of engineering performance and testing, the design should [15,16]:

- demonstrate availability and integration of essential fusion technologies like superconducting magnets and remote handling
- test components for a future reactor
- test tritium breeding module concepts;
- Test high heat flux components with a 14 MeV-neutron power load on the first wall  $> 0.5 MW/m^2$  and fluence  $> 0.3 MWa/m^2$  .

In addition, the device should [15,16]:

- use as far as possible technical solutions and concepts developed and qualified during the previous period of the EDA, fulfilling all previous demands, but
- cost about 50% of the direct capital cost of the 1998 ITER Design.

#### 2.4.4 Program

The program of the ITER tokamak is divided into several phases, building up to full load operation with Deuterium-Tritium fuel.

##### H Phase [16]

This is a non-nuclear phase using only hydrogen or helium plasmas, planned mainly for complete commissioning of the tokamak system in a non-nuclear environment where remote handling maintenance is not required. It enables simulating parts of the DT phase, without activating the reactor allowing for changes. Electromagnetic loads due to disruptions or vertical displacements will be comparable to those in the DT phase. Also the heat loads on the divertor will be comparable, yet slightly lower.

It does however not enable full testing due to lower heat content of the plasma. Also will there be no high energy neutrons or alpha particles, meaning that neutron flux resistance cannot be tested.

The length of the H phase depends on its success and its impacts on the DT phase in particular on the ability to achieve good H mode confinement with a suitably high plasma density.

##### D Phase [16]

The D phase is very similar to the DT phase. The main difference is a lower amount of alpha heating. Since some T will be created the beginning of the d phase will allow nuclear commissioning and the shielding performance can be tested. The D phase will allow simulating of reference DT operational scenarios.

##### DT Phases [16]

The DT phases represent the main part of the operation of ITER.

During the first one fusion power and burn pulse length will gradually increase until the goals are reached. Targets are developing of steady state operation, testing of DEMO relevant blanket modules.

The second DT phase will see full DT operation while trying to improve overall

performance. This is coupled with testing of high neutron fluence components and materials. It also addresses issues of improved modes of operation. A decision on a tritium breeding blanket during the the second DT phase will be made based on Tritium availability from external sources, its relative cost, the results of breeder blanket module testing, and experience with plasma and machine performance.

## 2.5 Divertor

### 2.5.1 General Description

The divertor is a region of the plasma where the outer magnetic field lines are opened (join up with the wall or a different part of the vacuum vessel) (see Figure 8). The X-point is created by applying a current below the plasma in the same direction as the plasma current. As a result the outer layers of field lines do not join up with themselves but are diverted onto the divertor target. The last closed surface of field lines is called the separatrix. Any particles inside the separatrix are well confined and can potentially take part in fusion reactions. All particles crossing the separatrix due to drifts or collisions are quickly directed onto the divertor plates and lost. This way the charged particles are kept from approaching the main wall.

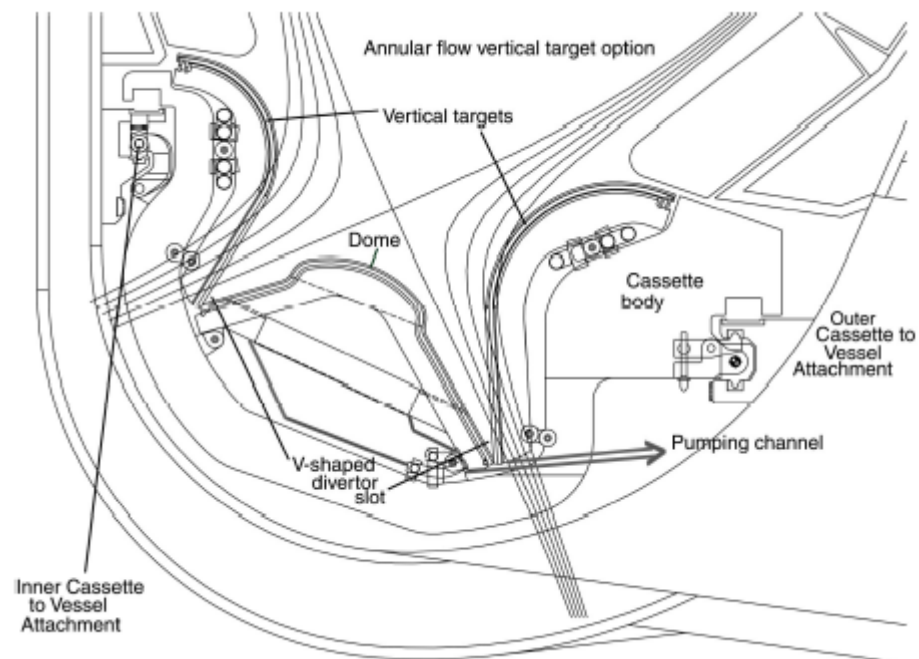


Figure 8: Cross-section through the divertor [8]

However the plasma facing components (PFC) of the target plates have to withstand all the heat and particle flux falling onto them.

## 2.5.2 Components and their Function

The divertor as a whole serves to exhaust the biggest part of alpha particle power, He ash and impurities from the plasma.

It is made up of 54 cassettes bodies (one shown on Figure 9), on which the other components are mounted. The cassette bodies provide basic shielding to the vessel and the magnets near the divertor [8]. They are mounted on rail in the vessel floor allowing them to be serviced through remote handling. This is a very important part of the ITER philosophy, as the divertor is one of the parts which are expected to be upgraded and/or changed several time during the lifetime of the machine [8].

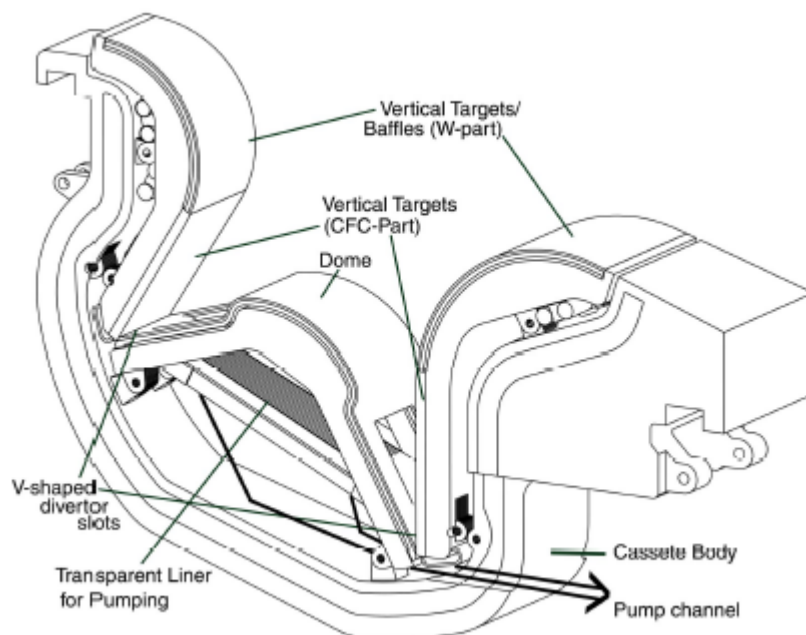


Figure 9: Divertor cassette [8]

The inner and outer vertical Targets are the main plasma facing components (PCF). They are inclined with respect to the poloidal field (see Figure 8) to spread the incoming power over a larger area. The lower part of the vertical targets directly interacts with the scrape-off layer (SOL) of the plasma. The upper part, the baffles, act as protection against neutrals. The surface of the target is cut up into tiles 20 mm by 20 mm with gaps between them allowing for thermal expansion due to high heat loads.

The private flux region with the dome is the area with no direct connection to the main plasma. There the pump channel is located which serves the purpose of removing any particles, that are no longer needed or wanted in the vessel.

### 2.5.3 Choice of Armor Materials

CFC and Tungsten are the materials used for the ITER divertor. Both materials have positive and negative properties.

Carbon-fiber composite (CFC) is forgiving as an armor material. It can take high heat loads due to good conductivity. If overheated during disruption events it will ablate and there is no concern over the behavior of a melt layer. Use of CFC also reduces problems in case of divertor misalignment, should the leading edges intercept the SOL (Flux around  $100\text{MW}/\text{m}^2$ ). [8].

For these reasons it has been chosen as the reference armor of the strike point regions.

However Carbon tends to form strong chemical bonds with Hydrogen. This could lead to large amounts of Tritium accumulating in dust in the divertor region at an estimated rate of  $5\text{g}$  (+/- 50%) T/pulse of 400s. This does not play a role during the start of ITER operations, since in the H phase no Tritium should be in the plasma.

Tungsten has been chosen as armor material for all other plasma-facing surfaces of the divertor, for the baffle regions of the target and the surface of the dome [8]. because of its high Z it has a lower splutter yield that Carbon and Tritium retention is not a big issue as W hardly bonds with Hydrogen. It also has a high melting temperature and specific heat capacity. It is not quite clear how a melt layer would react to the electromagnetic forces and how much of the melt layer would be lost. High Z materials like W can also not be tolerated in such concentration like C in the plasma core as they would radiate off too much of the plasma's energy.

If the H phase shows that the loads on the divertor can be handled by an all Tungsten divertor CFC will most likely not be used for any PFC. The maximum T inventory of ITER part of the nuclear licensing conditions and a W divertor would drastically reduce Tritium accumulation in the vessel.

## **2.6 Edge Localized Modes (ELMs)**

ELMs are instabilities that occur in plasmas that are in high confinement mode (H-mode), in which the plasma builds up a transport barrier. This leads to a large gradient of pressure and temperature. Due to this pedestal the energy content of the plasma and its confinement are dramatically improved. However, when this gradient builds up, there is a regular (pseudo-periodic) relaxation. This is called an ELM. During an ELM event large amounts of particles (carrying energy) leave the plasma.

With decreasing ELM frequency, their amplitude becomes larger and their effect on the divertor can become devastating. There is research under way how to artificially trigger ELMs before they can build up, or how to suppress them totally.

It is believed [1] that during ELMs in ITER the energy flux heading mainly to the divertor is too strong and too rapid for any target material to withstand it. Pessimistic estimations see them so devastating, that only few days of ITER operation with ELMs will be possible. On the other hand there are optimistic predictions of several years until the divertor would need to be changed. This thesis concerns exactly this uncertainty.

## **3 Simulation of the Heat Conduction**

### **3.1 Motivation**

The motivation of studying the heat conduction in the divertor is simple. Since the divertor is serving as an exhaust for the fusion products (helium ash) and the magnetic field lines are opened there to serve this purpose, it is natural, that during plasma instabilities (especially ELMs) the highest flux of particles (with high energies) will hit exactly the divertor desks. Such high amounts of heat can cause a high amount of potential damage to the divertor cassette. The damage can be in the form of increased material erosion, such as melting (in the case of a tungsten divertor) or evaporation (if carbon is used for the target). One of the two biggest dangers connected with such erosion are heavy particles entering the plasma and cooling it down to such a degree that the efficiency of the overall operation will drop significantly. The second problem is the need for regular repairs, which would slow down the research timetable of the whole facility. These reconstructions also would consume many resources.

Since there is no tokamak in operation with a comparable size and specification like ITER, there are no experimental data available and it is logical that a computer simulation is the best way to get an overview of what could be the best solution the problem faced. In this case the simulation should help to decide whether tungsten can be used for the divertor or if CFC should be used. Both materials have advantages and disadvantages.

The biggest disadvantage of CFC is the high tendency of carbon to form strong chemical bonds with hydrogen. Since the plasma inside the tokamak will contain a considerable amount of radioactive tritium, this would cause the divertor to become radioactive over time, causing significant trouble during maintenance. Therefore it is believed that future commercial reactors operating in steady state condition must contain no Carbon at all. On the other hand CFC has a very good heat conductivity, reducing the risk of destruction by overheating. That is the reason almost all current tokamaks use graphite for their PFCs.

Tungsten does not easily bond with any of the light particles from the plasma and is therefore the more preferred material for the divertor target. It also has a high specific heat

capacity. Unfortunately its heat conductivity is relatively poor. Further Tungsten is a relatively heavy metal and any particles entering the plasma would cause high energy losses through radiation. Despite that it is a more favorable material due the lower risk of tritium retainment. If the simulation would confirm its stability under the high loads, the need for CFC would be drastically reduced and a Tungsten divertor would be probably the best solution for the DT phase of ITER operations.

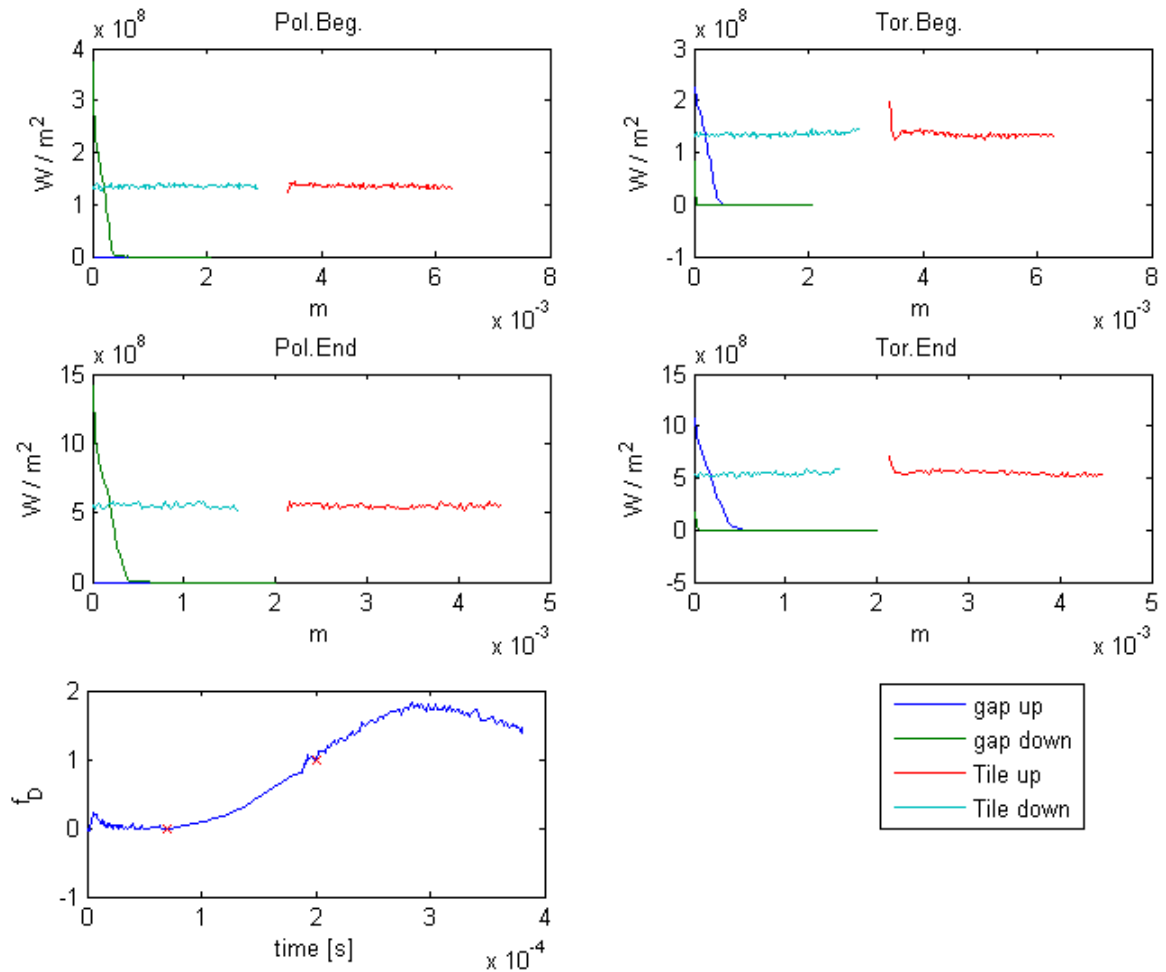
### **3.2 Input from other Simulations**

As input data two independent simulation outputs were combined.

The first one [2] gave the total flux density as a function of time during an ELM. The second simulation [3] served to give the spacial distribution of the income flux of particles. Combining both gave the distribution  $P$  of the flux on the target tile as a function of 3 space dimensions and time.

The model [2] is based on one-dimensional kinetic simulations of the parallel transport (along magnetic field) of an ELM in the JET SOL nearby the separatrix. In [2, Fig.6], simulation for ITER is presented. The function

At two points in time within this ELM evolution, symbolically called Beg. and End (of ELM), another Particle-In-Cell model [3] solves power flux in the ITER divertor tile gaps. It shows that the power flux does not hit the divertor only in a radial-toroidal direction, but also to also with a substantial poloidal component. This comes from electromagnetic interaction of the plasma with the divertor. Since PIC simulations are demanding on CPU time only a few time-points can be simulated. Since a full time and space distribution is needed as input to our 3D model, we perform simple interpolation between these two cases, based on function  $f_D$ . This means a smooth (in time) transition between the two space distributions the absolute value of the flux changing strongly with time given by the kinetic model [2].



D.Tshakhaya: non-linear power flux transfer.  $Q=Q_b+(Q_e-Q_b)*f_D$  between beginning and end of ELM

Figure 10: Input data for the simulation of ELM related fluxes. The four upper graphs show the flux into poloidal and toroidal gaps between tiles at the beginning and the end of an ELM. The lower graph gives the function with which interpolation is performed between these two distributions.

On Figure 10 an overview over the input data is given. The flux distributions in the gaps were simulated for two points in time during the build up of an ELM [2]. The function  $f_D$  allows us to make an interpolation between those two points (marked x) and extrapolate until the end of the ELM. The labels “gap up” and “gap down” denote the radial profile of the flux falling onto the side walls of the tile on either side of a gap. “Tile up” and “Tile down” represents the flux falling onto the top surface of the tiles near the gap. Figure 11 summarizes the distribution at the very beginning of the ELM simulation.

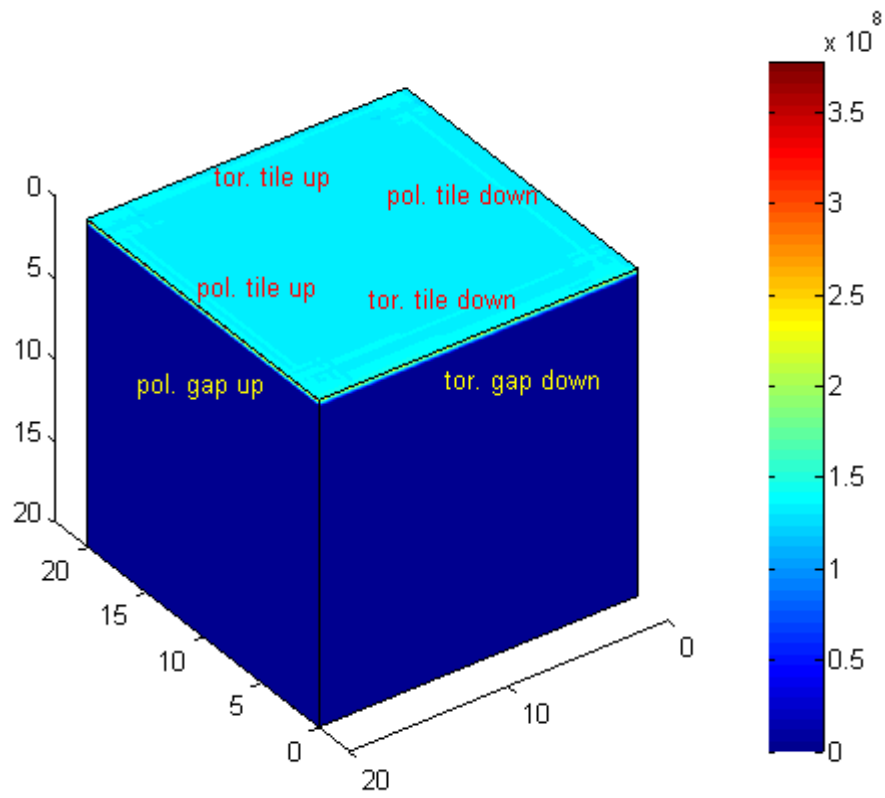


Figure 11: Flux distribution over the tile. Units on the color bar are  $W/m^2$

### 3.3 The Model

#### 3.3.1 Maths Behind the Model

The tile is divided into an equally spaced grid. The resolution of the grid can be varied. This creates a fixed number of cells to work with. Within these cells the temperature is considered to be constant and the cell is represented by the point in its center. This way the continuous problem is reduced to the problem of a finite number of point temperatures with fixed distances. The heat flux  $Q$  is calculated from the temperature distribution  $T(x,y,z)$  using the formula

$$Q = -\lambda \cdot \text{grad } T \quad , \quad (2)$$

where  $\lambda$  is the heat conductivity ( $\text{J m}^{-1} \text{K}^{-1} \text{s}^{-1}$ ) of the material. The change in temperature over time is then given by the formula

$$\frac{\partial T}{\partial t} = \frac{1}{c \rho} \text{div } Q \quad , \quad (3)$$

where  $c$  is the heat capacity ( $\text{J kg}^{-1} \text{K}^{-1}$ ) and  $\rho$  the density of the material. For materials with a scalar heat conductivity (like Tungsten) these equations can be combined into the heat equation

$$\frac{\partial T}{\partial t} = \frac{\lambda}{c \rho} \Delta T \quad , \quad (4)$$

where  $\Delta$  is the Laplace operator. But even with a scalar conductivity, it is useful to evaluate equation (2) first and combine the resulting flux with the incoming flux from the plasma. This way equation (3) describes both the heating of the surfaces as well as the diffusion of temperature inside the material. A further advantage is, that this way no second order derivation needs to be evaluated as would be required in equation (4).

The first derivative with respect to space variable  $x$  ( $y$  and  $z$  analogically) is evaluated in the center point between two adjacent cells:

$$\left( \frac{\partial f}{\partial x} \right)_{(i+\frac{1}{2}),j,k} = \frac{f_{(i+1),j,k} - f_{i,j,k}}{dx} \quad , \quad (5)$$

where  $dx$  is the size of the spacial step linked to the index  $i$ . Indexes  $j$  and  $k$  correspond to axis  $y$  and  $z$  respectively. If the grid would not be equally spaced,  $dx$  would be a function of the index  $i$ . As this would lead to a large number of matrix operations, the idea of an inhomogeneous grid was abandoned in favor of the more simple model, allowing faster running of the program even at a high number of cells.

### 3.3.2 Verification of the Model

As the main verification for the model we used the analytical solution for surface heating [6] for a tile with the same geometry. Analytically a constant power flux causes a surface to heat up proportionally to the square root of time:

$$\delta T_n = \frac{2q_n}{k} \sqrt{\frac{\kappa t}{\pi}} \quad (6)$$

Here  $\kappa = k / (\rho C_p)$ , where  $k$ ,  $\rho$  and  $C_p$  are the heat conductivity, density and specific heat respectively.  $q_n$  is the surface flux and  $t$  is the length of time the material is heated. As a reference value  $q_n = 100 \text{ MW m}^{-2}$  and  $t = 1 \text{ ms}$  was chosen. The change of temperature  $dT$  should be 172.54 K for CFC and 168.21 K for Tungsten. Table (1) shows how close our model gets to these values using different resolutions  $dl$ . It is visible that for CFC a resolution of 0.1mm is enough to achieve less than 1% error. For Tungsten achieving a similar precision requires nearly double the resolution so 0.05mm.

This difference can be explained by comparing the conductivity of both materials. In radial and poloidal direction CFC has nearly double the conductivity (324 compared to 174  $[\text{W/m}\cdot\text{K}]$ ) These resolutions are used in all further simulations of time dependent fluxes. That means 0.1mm of radial resolution for CFC and 0.05mm for W.

$dl$ [m]	dT CFC	dT W
1.00E-3	98	55.5
5.00E-4	105.7	98.8
2.50E-4	164.5	141.9
1.67E-4	168.9	155.7
1.25E-4	170.5	161.1
1.00E-4	171.3	163.6
6.67E-5	172	166.2
5.00E-5	172.2	167.1
2.50E-5	172.3	167.9
<b>analytical</b>	<b>172.53</b>	<b>168.21</b>

Table 1: Testing of the model, using a constant power flux density for a fixed time and a variable space step  $dl$  in radial direction

## 3.4 *Technical Details of the Program*

### 3.4.1 *Parameters and Observed Quantities*

The main parameters of the simulation are the material (with all its material constants), the space step in each direction and the time step.

The material parameter only takes two values representing CFC and Tungsten, but other materials can be easily added by extending the file containing the material constants.

The maximum resolution is limited by the RAM memory which Matlab can allocate. In our case it is a maximum of 500 MB. Fortunately this is just enough to satisfy the needs we found in Table 1. The time step is linked to the spacial resolution by a factor of numerical stability  $NS$  (as defined by (7)) that has to be smaller than  $1/2$  [20]. In our code a factor of  $1/6$  is usually used.

$$\frac{1}{2} \geq NS = \frac{\lambda}{\rho c} \cdot \frac{dt}{dl^2} \quad (7)$$

This means that a finer grid also requires a smaller time step. Fast processes such as ELMs therefore need to be simulated with a high resolution, while slowly changing processes like the nearly constant flux between ELMs can be simulated with a substantially lower resolution and longer time step.

During the simulation several physical quantities of interest are calculated. Firstly, the surface and edge temperatures are extrapolated from the points representing the elements under the surface. From these temperatures the surface cooling effects (radiation, sublimation and melting) are evaluated. The maximum and average temperature of the tile are recorded and shown in a graph. The surface temperatures are represented by colors on a 3D graphical representation of the tile. A second graph shows the temperature distribution along the edges of the tile. From regular screen shots during the simulation an animation can be created.

Since the effects of sublimation and melting are not only of a cooling nature but also cause loss of material their rate also recorded. From the integral of these functions the total amount of material, that changed state, can be calculated.

### 3.4.2 Boundary Conditions

To get the best results, it is important that all the inputs are as close to reality as possible. This does not only concern the fluxes, as described earlier, but also the temperature distribution on the divertor tile before the ELM occurs. As the length of an ELM is very short compared to the time the plasma is in stable H-mode it is logical to assume that between ELMs the divertor returns to a “basic” temperature distribution. This will be mainly determined by the flux falling on the divertor, which is estimated to be  $5\text{MW}/\text{m}^2$  [1] in perpendicular direction to the tile.

A complete simulation cycle contains 4 steps. Before the first step the divertor is considered cold. This means a uniform temperature of 414K (estimated temperature of the cooling liquid at the inner vertical target during operation) [8]. The first step simulates the flux during a normal H-mode ( $5\text{MW}/\text{m}^2$ , see above) to obtain an initial temperature gradient before the first ELM. The heating due to this ELM is simulated in the second step. The third step is again considering only H-mode flux levels and gives an insight into the cool down phase. The fourth and last phase is the next ELM and the results obtained during this phase are considered final. For verification purposes steps 3 and 4 can still be repeated as steps 5 and 6. The results should be identical to those obtained in steps 3 and 4. Indeed the temperature after each “cool down” was identical, even though the second ELM heated the tile slightly more than the first one.

### 3.4.3 Implicated Cooling Mechanisms

One of the most basic phenomena that needs to be considered when heating a material to high temperatures is radiating like a black body. The amount of energy lost depends on the surface temperature and the process cools the surface of the divertor. Not considering this effect would therefore cause a more pessimistic result (higher temperature and higher erosion). According to the Stefan-Boltzmann law the power  $P$  emitted by the area  $A$  of absolute temperature  $T$  is equal to

$$P = \sigma AT^4 \quad (8)$$

where  $\sigma = 5.67 \times 10^{-8} \text{W m}^{-2} \text{K}^{-4}$  is the Stefan-Boltzmann constant. Since both Tungsten and CFC are not “absolutely black” materials, gray body has to be considered instead. This

means multiplying the right hand side of the Stefan-Boltzmann law (8) with the emissivity  $\epsilon$  of each material.

$$P = \epsilon \sigma A T^4 \quad (9)$$

For Tungsten this is 0.25 [19], for CFC values around 0.85 can be used. The exact value depends on the manufacturer.

In the simulation this radiation is applied after the heat has diffused. The change of temperature in each surface cell therefore is equal to

$$\Delta T = \epsilon \frac{\sigma T^4 dt dA}{\rho C_p dV} = \epsilon \frac{\sigma T^4 dt}{\rho C_p dR}, \quad (10)$$

where  $dR$  is the thickness of the surface layer from which the material radiates,  $C_p$  is the heat capacity and  $\rho$  the density.

Another important factor is the built-in active cooling system of the divertor. Cooling pipes run 20mm below the divertor tile surface [4]. During a single ELM this is too far to have a direct effect on the surface temperature since the heat does not penetrate more a couple of millimeters below the surface during the short duration of an ELM event. The exact cooling mechanism therefore is not a high priority in the simulation. For purposes of simplicity cooling is implemented by just keeping the area 20 mm below the surface at a constant temperature, the temperature of the coolant (410 K at the high field side strike point [8]), but for uncertainties how the coolant removes the heat from the block, it is not set to 410 K but 500 K.

Another way to cool the surface directly is change of state of the material. For CFC this would be sublimation, in the case of Tungsten melting. These are material-specific issues and are described in further details in the following two sections.

#### 3.4.4 Issues for Simulating Tungsten

Tungsten is a metal and as such it has a homogeneous structure without a dominant axis along which it would conduct heat better or worse.

Tungsten melts at a temperature of 3683 K [7]. During the process of melting the

temperature will not exceed this point. Any additional thermal energy is used to melt more material. Melting was implemented only virtually. The heat of melting for Tungsten equals  $h_m=33.7\text{ kJ/mol}=0.2057\text{ MJ/kg}$  [7]. For simplicity, at no time in the simulation any cell contains information about how much material has melted. The change of material properties is not simulated either. This could be implemented in the future. Each cell behaves like it was still completely solid. In practice that means keeping the temperature at a maximum of 3683 K and keeping only a record of the rate of melting for the whole object as well as its integral function. During an ELM, if melting is not simulated, the surface temperature only rises. This means that in this phase of the simulation no solidification can occur. Solidification is hence only an issue during the cool down phase between ELMs. It should, however, occur right after the ELM and the effect is minimized through the long period of the cool down compared the ELM itself.

### 3.4.5 Issues for Simulating CFC

CFC is an artificial material made from Carbon strings in which carbon atoms are arranged in a crystal structure along a major axis. It has different conductivities in the directions parallel to this axis and perpendicular to it. In the perpendicular directions the conductivity is higher (  $324\text{ W m}^{-1}\text{ K}^{-1}$  ) than in the parallel direction (  $86\text{ W m}^{-1}\text{ K}^{-1}$  ). For this reason alignment is a very important factor. To achieve a high conductivity away from the divertor surface (in the radial direction), the material axis is parallel to the divertor tile surface. The alignment of the material axis with respect to the toroidal and poloidal coordinates is given as follows. The axis of the material runs parallel to toroidal axis of the tokamak meaning that the tile has a lower conductivity in this direction than in the poloidal one, which is perpendicular to the material axis.

Like normal carbon, CFC sublimates when heated sufficiently. The particles lost due to sublimation are free and can be pumped away by the cryopump. But they can also accumulate in the tile gaps as dust, a major issue when considering Tritium retainment. Important however is the small probability of particles condensing on the surface of the tile, where this process would release energy. The destruction of the tile itself and the behavior of the carbon particles after sublimation is therefore not simulated. The program only evaluates how much material would be lost, the mass of the simulated tile however does not change

during the simulation. This is due to the assumption that the amount of material lost during one ELM is by several orders of magnitude smaller than the mass of the tile itself. The only effect of the sublimation in the simulation will be cooling. The rate of material loss due to sublimation is temperature dependent [4]:

$$\dot{n}_{subl} = \frac{2.6 \cdot 10^{26}}{\sqrt{M T}} 10^{B-A/T} \left[ \frac{Atoms}{m^2 s} \right], \quad (11)$$

where M is the atomic mass (12AMU for carbon in this case), T the temperature (in Kelvin). The parameters A and B describe the behavior of the vapor pressure of the material. For the combination of the species C<sub>1</sub>, C<sub>2</sub> and C<sub>3</sub> the values are  $A=40181$  and  $B=14.80$  . [4]. The strong effect of slight temperature changes can be seen on Figure 12. At 2200K the sublimation rate is only  $0.01 \text{ mg m}^{-2} \text{ s}^{-1}$  , At lower temperatures sublimation is not a very dominant factor, especially not for processes much faster than 1 s. At 3000 K this rate is 10 000 times bigger and already needs to be taken very serious.

The cooling effect is given by the latent heat of evaporation  $h_{evap} = 715 \text{ kJ/mol} = 59.6 \text{ MJ/kg}$  for CFC.

$$q = \dot{m}_{subl} \cdot h_{evap}, \quad (12)$$

where q denotes the amount of heat lost [  $W/m^2$  ] and  $\dot{m}_{subl}$  is the mass loss rate [  $kg m^{-2} s^{-1}$  ] . It can be calculated by dividing the result from (11) by Avogadro's number ( $6.022 \cdot 10^{23} \text{ atoms/mol}$ ) and multiplying with the atomic mass ( $0.012 \text{ kg/mol}$ ) .

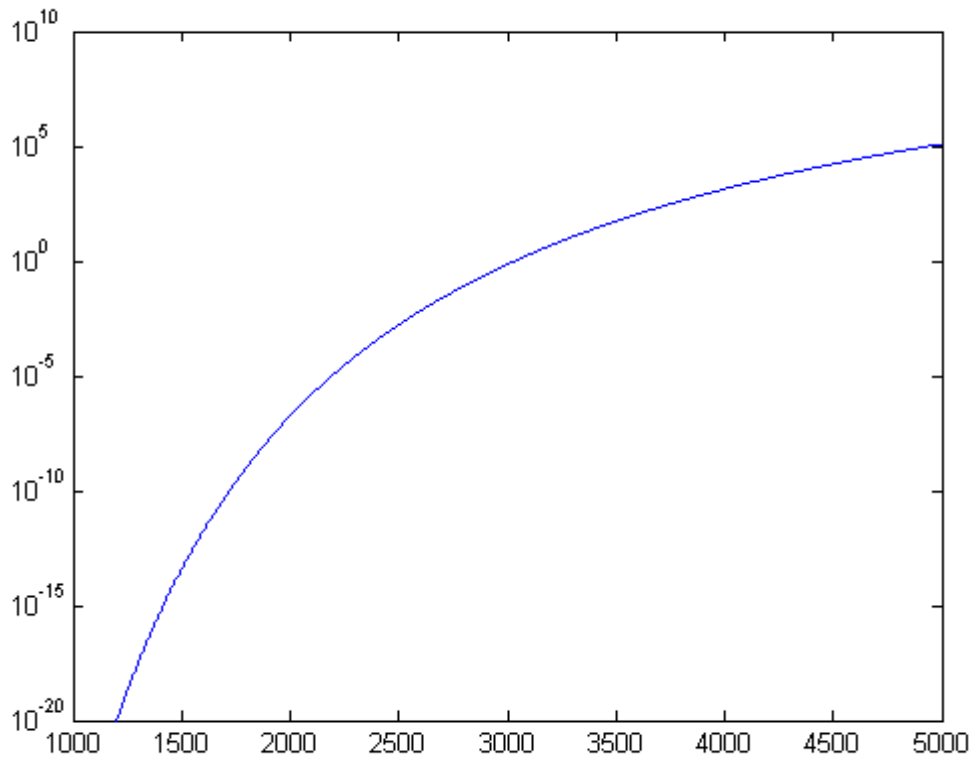


Figure 12: Dependency of sublimated mass (y axis) from a CFC surface in  $g m^{-2} s^{-1}$  on temperature (x axis) in K

## 3.5 Results

### 3.5.1 Tungsten

After cooling down the maximum surface temperature was 861 K (see Figure 13).

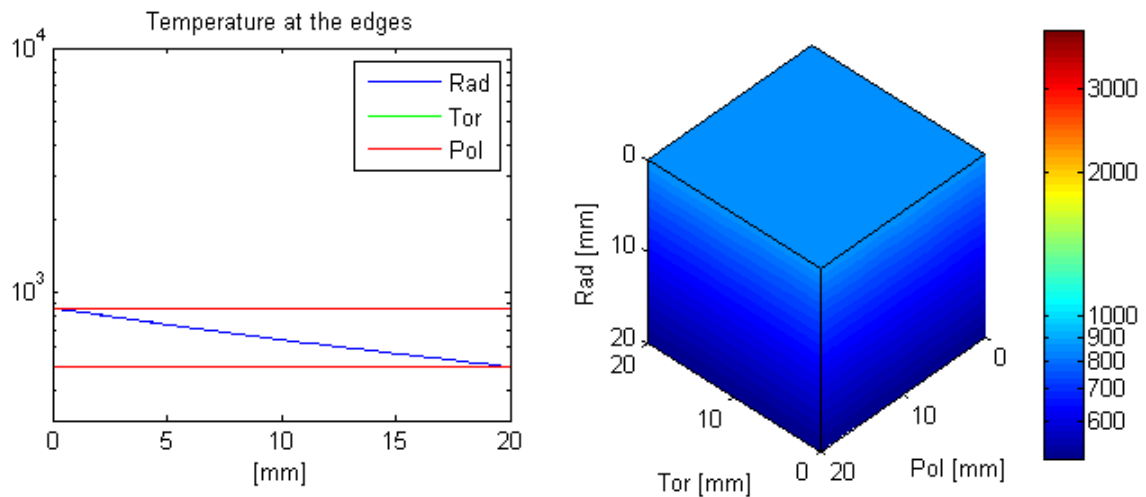


Figure 13: Temperature profile of the W divertor after cooling down

During the ELM the surface temperature of the W tile rises to 1840 K, at the edges it is as much as 2911 K. The change of maximum temperature is seen in Figure 14. The minimum temperature represents that of the coolant and is graphed as a reference value. It is clearly visible that the average temperature hardly changes, while the maximum temperature (at the corner of the tile) grows by about 1500 K within only 0.2ms. The effects of the ELM do not even reach 1mm into the tile, but due to the high heat capacity of W the melting temperature is not even reached. That means that if ELMs do not turn out stronger than in this simulation, the heat loads will not be responsible for the destruction of a W divertor.

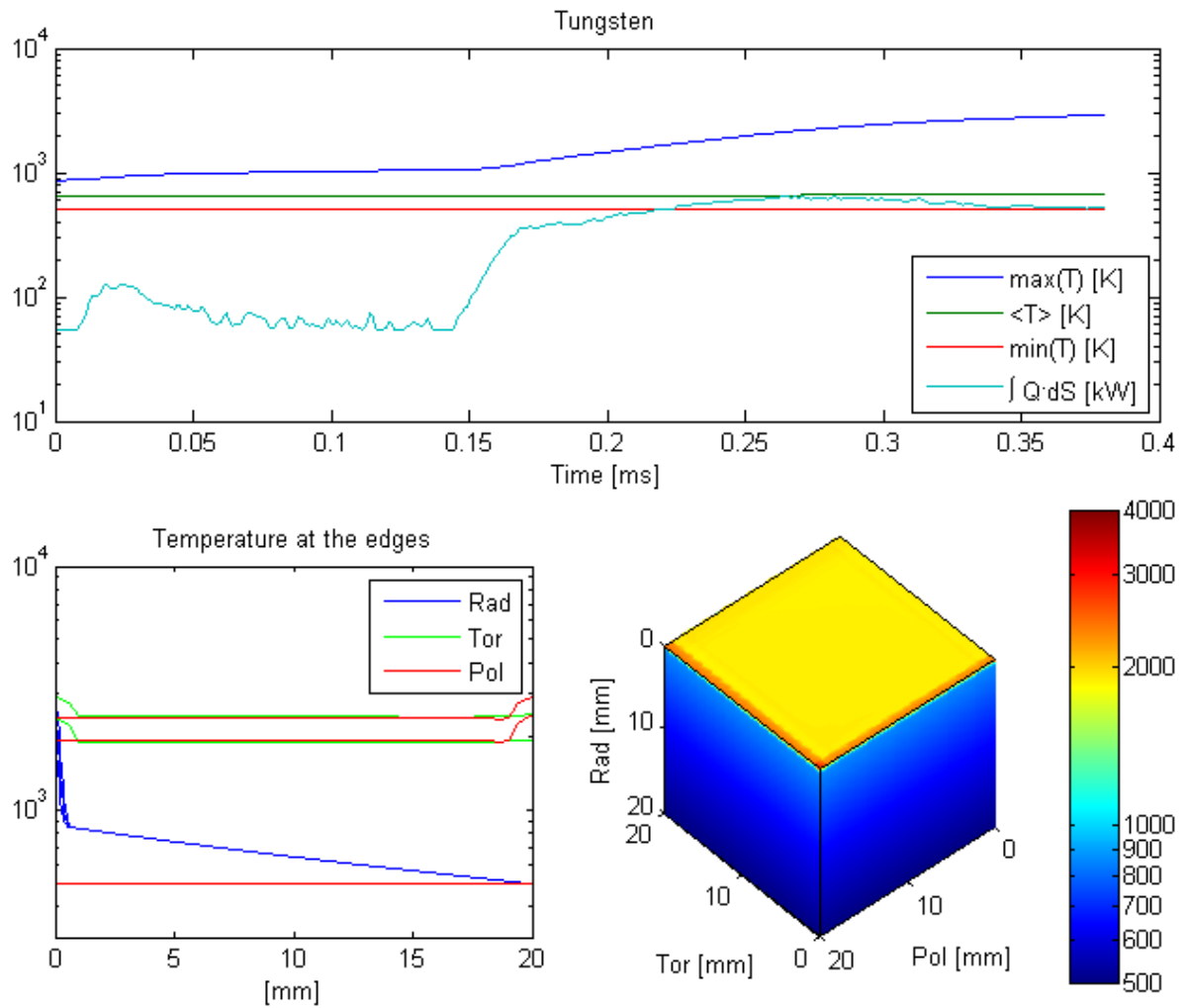


Figure 14: Simulation results for the ELM on a W tile. The bottom right shows a 3D-model of the tile to a depth of 20mm. The color represents the temperature. The graph left to it shows the temperature profile along the edges. The top graph shows the maximum and average temperature changing with time and the power of the ELM

### 3.5.2 CFC

Temperature:

Before the ELM the maximum temperature was 783.1 K.

During the simulated ELM the temperature rises to a maximum of 2942 K. The change of maximum and average temperature can be seen in Figure 15. The minimum temperature represents that of the coolant and is graphed as a reference value. It is clearly visible that the average temperature hardly changes, while the maximum temperature (at the corner of the tile) grows by over 2000 K within only 0.38ms. The ELM is so fast that it only affects 1.5 mm thickness of the tile.

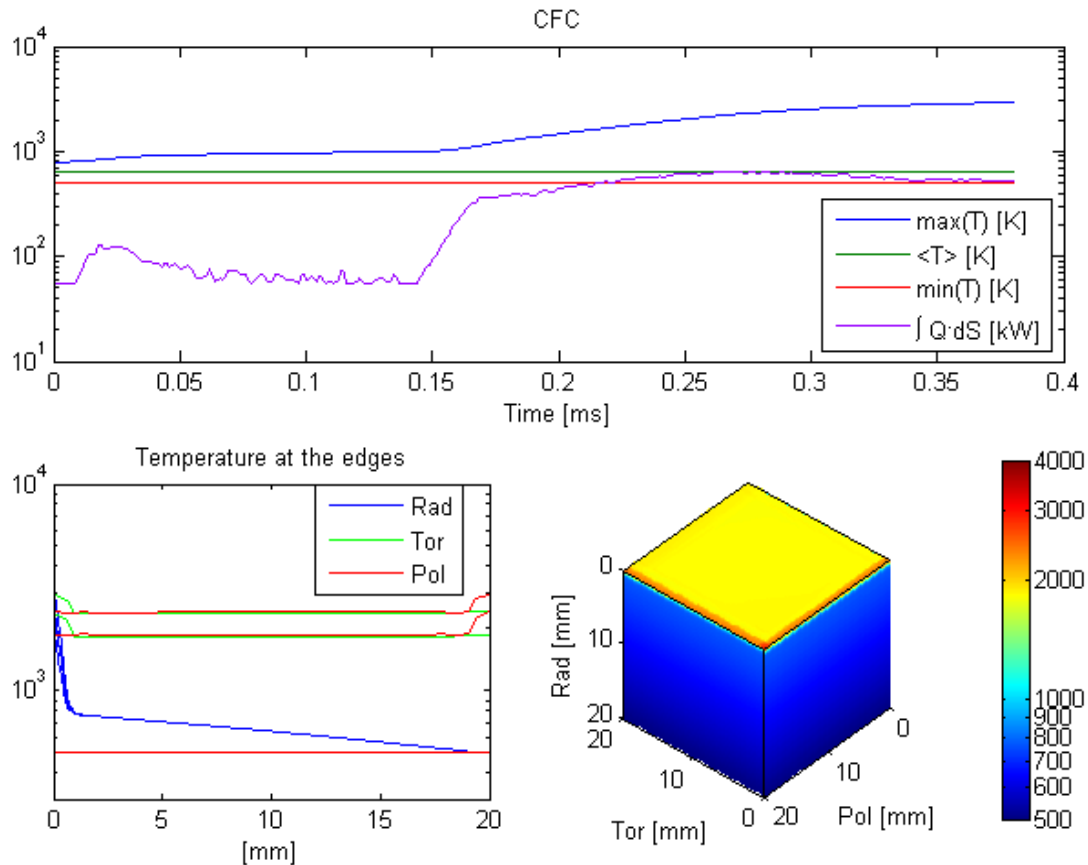


Figure 15: Simulation results for the ELM on a CFC tile. The bottom right shows a 3D-model of the tile to a depth of 20mm. The color represents the temperature. The graph left to it shows the temperature profile along the edges. The top graph shows the maximum and average temperature changing with time and the power of the ELM

Sublimation losses:

The simulation indicated that during one ELM a total of only 0.17  $\mu\text{g}$  (see Figure 16) is sublimated from each tile. This accounts for only 0.4  $\text{ng}/\text{m}^2$  or 935 pm thickness of the tile. To erode 1mm from a CFC divertor target it would take therefore 1.07 million ELMs, which is in the order of 2000-2500 pulses (length around 400s, ELM frequency 1 Hz). Since the rate of sublimation is a function rapidly increasing with growing T (see equation (11)), it can be assumed however that almost all of the sublimation takes place at the corner facing to the front in Figure 15. After some time this corner will be strongly eroded and the effect should reduce to its flattening.

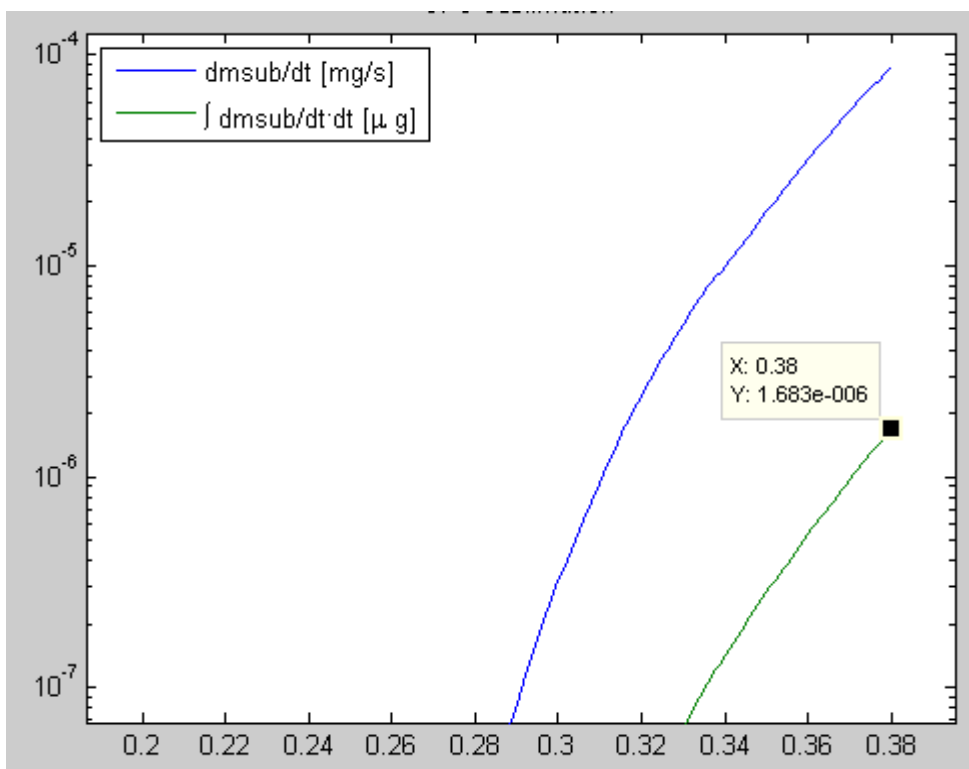


Figure 16: Change of sublimation losses over time (x axis), showing only the end of the ELM. The blue line ( $dmsub/dt$ ) shows the rate of sublimation, the green line shows the accumulated losses. The marker denotes the final value at the end of the simulation.

### **3.5.3 Comparison**

While CFC loses only about 1 nm of material per ELM, which is extremely good news but Tungsten does not even get near its melting temperature.

From the temperature profiles along the edges (Figures 14 and 15) it can be seen, that CFC does indeed conduct the heat away quicker, but its lower heat capacity still makes it more vulnerable to high heat loads than W.

### **3.6 Summary**

As part of this work the heat conduction within an ITER tile was simulated using a Matlab code. Once W was the material and once CFC. The flux distribution was taken by merging the results of a kinetic and a PIC simulation.

The W tile performed better under ELM conditions heating up less than its CFC counterpart. CFC did not show dangerous erosion, but the effect of sublimation could be much stronger if the ELM would be only a few percent more intensive

### **3.7 Implications**

Given that the simulation showed light erosion for the CFC tile but no erosion at all for the W tile, it is not difficult to make a conclusion. Tungsten is a suitable armor for the PFC of the ITER divertor and should be favored over CFC, due to other factors, such as its lower sputter yield and the big advantage of not bonding with Tritium.

The 1% of error in the code (see Verification of the model) is partly balanced by weaker cooling, but it has to be kept in mind, that any slight increase can still mean a lot more sublimated material from a CFC tile, further reducing its lifetime. Despite the W divertor still having reserves, the control over ELMs must be a priority in the ITER research program as further upscaled ELMs in DEMO cannot be accepted unless an even better material than Tungsten can be produced for its divertor.

Important is also to mention that the data for our ELM just stop after 0.38 ms. We assumed so far a very quick drop in fluxes after this time, but a longer lasting ELM could actually put CFC in favor again, since W does not conduct heat way quick enough. It accumulates near the surfaces and diffuses only slowly.

### **3.8 Possible Future Improvements**

At the moment the code is very simple and makes several assumptions that make its results slightly optimistic. It does however already consume literally all system resources available to Matlab. Before advanced physical phenomena can be implicated, the program itself needs to be adapted to use less RAM. This could be achieved by replacing some of the matrix operations by “for” cycles. Less arrays would need to be saved (3 arrays for fluxes, each the size of the grid itself could be freed), but the run time would most likely increase. On the other hand would this help to implicate a non constant resolution, where cells near the surface could be thinner than further inside.

Another option to save RAM is reducing the tile to its upper 5 millimeters during ELM event simulations, neglecting the cooling for a short time. This would cut RAM requirements by a factor of four.

No matter how RAM will be gained, phenomena that worth considering for implementation are:

- the actual erosion of the target, ie. changing its geometry during the simulation according the data gained so far.
- physical and chemical spluttering as implicated in [4].
- the interaction of the divertor tile with the cooling pipe and the coolant. It could be useful in order to learn something about the quality of the cooling system.
- the simulation of other scenarios like disruptions, if input data can be aquired.

## 4 References

- [1] R.A. Pitts. Material erosion and migration in tokamaks. Plasma Phys. Control. Fusion 47 (2005) B303-B322
- [2] D. Tskhakaya et al. Kinetic simulations of the parallel transport in the JET scrape-off layer. Journal of Nuclear Materials 390-391 (2009) 335-338.
- [3] R. Dejarnac et al. Power flux in the ITER divertor tile gaps during ELMs. Journal of Nuclear Materials 390-391 (2009) 818-821
- [4] E. D'Agata et al. A program to evaluate the erosion on the CFC tiles of the ITER divertor. Fusion and Engineering Design 82 (2007) 1739-1746
- [5] [http://en.wikipedia.org/wiki/Nuclear\\_fusion](http://en.wikipedia.org/wiki/Nuclear_fusion) (cit. 27.11.2010)
- [6] V. Thopson et al. Analysis and design of the beryllium tiles for the JET ITER-like wall project. Fusion Engineering and Design 82 (2007) 1706–1712
- [7] J. G. Stark, H. G. Wallace. Chemistry data book, second edition in SI (1982). ISBN: 0-7195-3951-x
- [8] ITER Technical Basis. Plant Description Document. G A0 FDR 1 01-07-13 R1.0
- [9] [http://en.wikipedia.org/wiki/Nuclear\\_binding\\_energy](http://en.wikipedia.org/wiki/Nuclear_binding_energy) (cit. 27.11.2010)
- [10] <http://en.wikipedia.org/wiki/Tokamak> (cit. 27.11.2010)
- [11] J. D. Ward. Fusion and the Future Energy Market. Presentation at the 47<sup>th</sup> Culham Plasma Physics Summer School, 12.-23. July 2010, Culham, UK.
- [12] Toni Johnson. Global Uranium Supply and Demand – Council on Foreign relations. [http://www.cfr.org/publication/14705/global\\_uranium\\_supply\\_and\\_demand.html](http://www.cfr.org/publication/14705/global_uranium_supply_and_demand.html) cit. 14.01.2010
- [13] N K Prasad et al. Challenges in the design of a prototype contactor assembly for the recovery of uranium from seawater. International Journal of Nuclear Desalination Volume 3, Number 3/2009, pages 241-246
- [14] ITER website: <http://www.iter.org/>
- [15] R Aymar et al. The ITER design. Plasma Physics and Controlled Fusion 44 (2002) 519-565
- [16] Summary of the ITER Final Design Report. July 2001. G A0 FDR 4 01-07-21 R 0.4
- [17] [http://www.iter.org/img/resize-725-90/www/edit/Lists/WebsiteText/Attachments/68/bg\\_tokamak.jpg](http://www.iter.org/img/resize-725-90/www/edit/Lists/WebsiteText/Attachments/68/bg_tokamak.jpg)
- [18] [http://www.anthonares.net/Fhsst\\_atomnucl6.png](http://www.anthonares.net/Fhsst_atomnucl6.png)

- [19] Tungsten properies. <http://www.tungsten.com/mtstung.html>
- [20] [http://en.wikipedia.org/wiki/Von\\_Neumann\\_stability\\_analysis](http://en.wikipedia.org/wiki/Von_Neumann_stability_analysis) (cit. 06.01.2011)

## 5 Acknowledgments

In first place, I would like to thank to my supervisor, Jan Horáček, whose kindness and patience helped me keep going even when the code seemed to develop more mistakes, every time I tried to fix one. Further thanks he deserves for his willingness to let me write this work in English, after all I am not sure if my knowledge of the Czech language would be sufficient yet for such a piece of work. Thanks also go to his colleague, Renaud Dejarnac, not only for providing data for the simulation, but also for his help in understanding them.

Secondly I want to thank my partner, Terezie, for her patience and support, through the whole time I was working and writing on this paper and my apology for the many days I was spending in front of the PC. Her motivation helped me in an unmeasurable way and without her I would not have managed.

And finally I would like to thank all those people who further contributed to this work, be it actively, or passively through their friendship making courses more bearable, leaving me more energy for this project.